ΛCDM and the Implications of the Hubble Tension

PhD Defence

June 28, 2022

George Alestas

Department of Physics, University of Ioannina
Website: georgealestas.github.io
g.alestas@uoi.gr

Publication Record

Cosmology Intertwined: A Review of the Particle Physics, Astrophysics, and Cosmology Associated with the Cosmological Tensions and Anomalies
E. Di Valentino et al., Contribution to the 2022 Snowmass Summer Study
JHEAp 34 (2022) 49-211
DOI: 10.1016/j.jheap.2022.04.002

Constraining a late time transition of G_{eff} using low-z galaxy survey data
G. Alestas, L. Perivolaropoulos and K. Tanidis
arXiv: 2201.05846, Supplemental Material

Late-transition vs smooth *H(z)* deformation models for the resolution of the Hubble crisis
G. Alestas, D. Camarena, E. Di Valentino, L. Kazantzidis, V. Marra, S. Nesseris and L. Perivolaropoulos
Phys. Rev. D 105, 063538
DOI: 10.1103/PhysRevD.105.063538, Supplemental Material

Hints for a gravitational constant transition in Tully-Fisher data
G. Alestas, I. Antoniou and L. Perivolaropoulos
Universe 7 (2021) 366
DOI: 10.3390/universe7100366, Supplemental Material

Late time approaches to the Hubble tension deforming *H(z)*, worsen the growth tension
G. Alestas, L. Perivolaropoulos
Mon.Not.Roy.Astron.Soc. 504 (2021) 3, 3956-3962
DOI: 10.1093/mnras/stab1070, Supplemental Material

A w – M phantom transition at z_t<0.1 as a resolution of the Hubble tension
G. Alestas, L. Kazantzidis, L. Perivolaropoulos
Phys.Rev.D 103 (2021) 8, 083517
DOI: 10.1103/PhysRevD.103.083517, Supplemental Material

Existence and Stability of Static Spherical Fluid Shells in a Schwarzschild-Rindler-anti-de Sitter Metric
G. Alestas, G.V. Kraniotis, L. Perivolaropoulos
Phys.Rev.D 102 (2020) 10, 104015
DOI: 10.1103/PhysRevD.102.104015, Supplemental Material

H_0 tension, phantom dark energy, and cosmological parameter degeneracies
G. Alestas, L. Kazantzidis, L. Perivolaropoulos
Phys.Rev.D 101 (2020) 12, 123516
DOI: 10.1103/PhysRevD.101.123516, Supplemental Material

Evading Derrick's theorem in curved space: Static metastable spherical domain wall
G. Alestas, L. Perivolaropoulos
Phys.Rev.D 99 (2019) 6, 064026
DOI: 10.1103/PhysRevD.99.064026, Supplemental Material

Publication Record

Cosmology Intertwined: A Review of the Particle Physics, Astrophysics, and Cosmology Associated with the Cosmological Tensions and Anomalies
E. Di Valentino et al., Contribution to the 2022 Snowmass Summer Study
JHEAp 34 (2022) 49-211
DOI: 10.1016/j.jheap.2022.04.002

Constraining a late time transition of G_{eff} using low-z galaxy survey data
G. Alestas, L. Perivolaropoulos and K. Tanidis
arXiv: 2201.05846, Supplemental Material

Late-transition vs smooth $H(z)$ deformation models for the resolution of the Hubble crisis
G. Alestas, D. Camarena, E. Di Valentino, L. Kazantzidis, V. Marra, S. Nesseris and L. Perivolaropoulos
Phys. Rev. D 105, 063538
DOI: 10.1103/PhysRevD.105.063538, Supplemental Material

Hints for a gravitational constant transition in Tully-Fisher data
G. Alestas, I. Antoniou and L. Perivolaropoulos
Universe 7 (2021) 366
DOI: 10.3390/universe7100366, Supplemental Material

Late time approaches to the Hubble tension deforming $H(z)$, worsen the growth tension
G. Alestas, L. Perivolaropoulos
Mon.Not.Roy.Astron.Soc. 504 (2021) 3, 3956-3962
DOI: 10.1093/mnras/stab1070, Supplemental Material

A w – M phantom transition at z_t<0.1 as a resolution of the Hubble tension
G. Alestas, L. Kazantzidis, L. Perivolaropoulos
Phys.Rev.D 103 (2021) 8, 083517
DOI: 10.1103/PhysRevD.103.083517, Supplemental Material

Existence and Stability of Static Spherical Fluid Shells in a Schwarzschild-Rindler-anti-de Sitter Metric
G. Alestas, G.V. Kraniotis, L. Perivolaropoulos
Phys.Rev.D 102 (2020) 10, 104015
DOI: 10.1103/PhysRevD.102.104015, Supplemental Material

H_0 tension, phantom dark energy, and cosmological parameter degeneracies
G. Alestas, L. Kazantzidis, L. Perivolaropoulos
Phys.Rev.D 101 (2020) 12, 123516
DOI: 10.1103/PhysRevD.101.123516, Supplemental Material

Evading Derrick's theorem in curved space: Static metastable spherical domain wall
G. Alestas, L. Perivolaropoulos
Phys.Rev.D 99 (2019) 6, 064026
DOI: 10.1103/PhysRevD.99.064026, Supplemental Material

Number of citations: ≈ 260
h-index: 9

Overview

What is the H_0 crisis?

- We consider the 2 basic methods of measuring the present value of $H(z)$:
  1. Using Cosmic Microwave Background (CMB) and Baryon Acoustic Oscillation (BAO) data.
  2. Using the distance ladder methodology, meaning SnIa calibrated from Cepheids (SH0ES) acting as standard candles.

What is the H_0 crisis?

- We consider the 2 basic methods of measuring the present value of $H(z)$:
  1. Using Cosmic Microwave Background (CMB) and Baryon Acoustic Oscillation (BAO) data.
  2. Using the distance ladder methodology, meaning SnIa calibrated from Cepheids (SH0ES) acting as standard candles.

- The first method produces,

$$H_0^{P18} = 67.36 \pm 0.54\, km\, s^{-1}\, Mpc^{-1} \tag{1}$$

What is the H_0 crisis?

- We consider the 2 basic methods of measuring the present value of $H(z)$:
  1. Using Cosmic Microwave Background (CMB) and Baryon Acoustic Oscillation (BAO) data.
  2. Using the distance ladder methodology, meaning SnIa calibrated from Cepheids (SH0ES) acting as standard candles.

- The first method produces,

$$H_0^{P18} = 67.36 \pm 0.54 \, km \, s^{-1} \, Mpc^{-1} \tag{1}$$

- While the second gives,

$$H_0^{R21} = 73.04 \pm 1.04 \, km \, s^{-1} \, Mpc^{-1} \tag{2}$$

N. Aghanim et al. (Planck), Astron. Astrophys. 641, A6 (2020)
A. G. Riess *et al.*, (2021), arXiv:2112.04510 [astro-ph.CO]

H_0 or M Crisis?

H_0 crisis might not be such an accurate term after all...

- The truth is that the tension might have very little to do with H_0 itself.

H_0 or M Crisis?

H_0 crisis might not be such an accurate term after all...

- The truth is that the tension might have very little to do with H_0 itself.
- We focus on M, the SnIa absolute peak magnitude.

H_0 or M Crisis?

H_0 crisis might not be such an accurate term after all...

- The truth is that the tension might have very little to do with H_0 itself.
- We focus on M, the SnIa absolute peak magnitude.
- The H_0 value given by the SH0ES distance ladder measurement is calculated indirectly by considering an inferred value of M from the Cepheid period-luminosity relation.

H_0 or M Crisis?

H_0 crisis might not be such an accurate term after all…

- The truth is that the tension might have very little to do with H_0 itself.
- We focus on M, the SnIa absolute peak magnitude.
- The H_0 value given by the SH0ES distance ladder measurement is calculated indirectly by considering an inferred value of M from the Cepheid period-luminosity relation.
- The problem is that that value of M was calculated for the redshift range $0.023 < z < 0.15$, therefore the H_0 value one gets from this method is a product of extrapolation.

H_0 or M Crisis?

H_0 crisis might not be such an accurate term after all...

- The truth is that the tension might have very little to do with H_0 itself.
- We focus on M, the SnIa absolute peak magnitude.
- The H_0 value given by the SH0ES distance ladder measurement is calculated indirectly by considering an inferred value of M from the Cepheid period-luminosity relation.
- The problem is that that value of M was calculated for the redshift range $0.023 < z < 0.15$, therefore the H_0 value one gets from this method is a product of extrapolation.
- This methodology is oblivious to any change in Physics below $z = 0.023$.

Adam G. Riess et al., Astrophys. J. 699, 539–563 (2009)

The S_8 or growth tension

- The Planck18/ΛCDM parameter values in the context of General Relativity seem to prefer stronger a growth of the cosmological perturbations than that indicated by the dynamical probes (*e.g.* weak lensing data).

The S_8 or growth tension

- The Planck18/ΛCDM parameter values in the context of General Relativity seem to prefer stronger a growth of the cosmological perturbations than that indicated by the dynamical probes (*e.g.* weak lensing data).
- The S_8 parameter is a combination of the parameters σ_8 and Ω_{0m} usually given by the relation $S_8 \equiv \sqrt{\Omega_{0m}/0.3}$.

The S_8 or growth tension

- The Planck18/ΛCDM parameter values in the context of General Relativity seem to prefer stronger a growth of the cosmological perturbations than that indicated by the dynamical probes (*e.g.* weak lensing data).
- The S_8 parameter is a combination of the parameters σ_8 and Ω_{0m} usually given by the relation $S_8 \equiv \sqrt{\Omega_{0m}/0.3}$.
- Most of the observations seem to indicate a value of S_8 that is at a 2 - 3σ level smaller than the $S_8 = 0.834 \pm 0.016$ value given by the Planck CMB measurement.

H. Hildebrandt et al., Mon.Not.Roy.Astron.Soc. 465 (2017) 1454
S. Joudaki et al., Astron.Astrophys. 638 (2020) L1

Do's and Don'ts regarding the tensions

- Consider all the available robust data (CMB, BAO, SnIa, *etc.*).

Do's and Don'ts regarding the tensions

- Consider all the available robust data (CMB, BAO, SnIa, *etc.*).
- Try to ease both of them simultaneously, two birds with one stone.

Do's and Don'ts regarding the tensions

- Consider all the available robust data (CMB, BAO, SnIa, *etc.*).
- Try to ease both of them simultaneously, two birds with one stone.
- Do NOT use a local H_0 prior.

Do's and Don'ts regarding the tensions

- Consider all the available robust data (CMB, BAO, SnIa, *etc.*).
- Try to ease both of them simultaneously, two birds with one stone.
- Do NOT use a local H_0 prior.
- If a prior is necessary make it an M prior instead.

The Two Paths to Follow

There are two schools of thought regarding the H_0 tension.

- The problem stems from systematic errors in the SH0ES calculations (*e.g.* Cepheid color-luminosity calibration systematics).

The Two Paths to Follow

There are two schools of thought regarding the H_0 tension.

- The problem stems from systematic errors in the SH0ES calculations (*e.g.* Cepheid color-luminosity calibration systematics).
- It is a gateway to new and exciting late and/or early time physics.

The Two Paths to Follow

There are two schools of thought regarding the H_0 tension.

- The problem stems from systematic errors in the SH0ES calculations (*e.g.* Cepheid color-luminosity calibration systematics).
- It is a gateway to new and exciting late and/or early time physics.

We will take the second (and most interesting) path, by considering a late time solution to the tension.

The Two Paths to Follow

There are two schools of thought regarding the H_0 tension.

- The problem stems from systematic errors in the SH0ES calculations (*e.g.* Cepheid color-luminosity calibration systematics).
- It is a gateway to new and exciting late and/or early time physics.

We will take the second (and most interesting) path, by considering a late time solution to the tension.

- We will consider a parametrization with a dark energy transition at ultra low redshifts ($z < 0.023$), coupled with a transition in the SnIa absolute magnitude.

E. Mortsell et.al., (2021), arXiv:2105.11461 [astro-ph.CO]
Perivolaropoulos, Leandros and Skara, Foteini, Phys. Rev. D 104 (2021) 12, 123511

Motivation

It seems quite clear that new physics are needed in order to resolve the tension.

Motivation

It seems quite clear that new physics are needed in order to resolve the tension.

Due to nature of the problem, a simple dark energy transition even though it allows H_0 to approach the value reported by SH0ES, fails to solve the problem by itself.

Motivation

It seems quite clear that new physics are needed in order to resolve the tension.

Due to nature of the problem, a simple dark energy transition even though it allows H_0 to approach the value reported by SH0ES, fails to solve the problem by itself.

Another type of modification is needed. A transition in M, the heart of the issue!

Questions to address

- Is the proposed model able to provide a satisfying resolution to the Hubble crisis, without worsening the growth tension?

Questions to address

- Is the proposed model able to provide a satisfying resolution to the Hubble crisis, without worsening the growth tension?
- Is there any observational evidence for such a parametrization and can it be observationaly constrained?

CMB Spectrum Degeneracies

We can uniquely describe the CMB temperature power spectrum by fixing a number of the following parameter combinations:

CMB Spectrum Degeneracies

We can uniquely describe the CMB temperature power spectrum by fixing a number of the following parameter combinations:

- The matter density parameter combination $\omega_{\rm m} \equiv \Omega_{\rm 0m} h^2$.
- The baryon density parameter combination $\omega_b \equiv \Omega_{\rm 0b} h^2$.
- The radiation density parameter combination $\omega_{\rm r} \equiv \Omega_{\rm 0r} h^2$.
- The primordial fluctuation spectrum and the curvature parameter $\omega_{\rm k} \equiv \Omega_{\rm 0k} h^2$.
- The flat universe co-moving angular diameter distance to the recombination surface

$$d_A(\omega_m, \omega_r, \omega_b, h, w(z)) = \int_0^{z_r} \frac{dz}{H(z)} \tag{3}$$

CMB Spectrum Degeneracies

We can uniquely describe the CMB temperature power spectrum by fixing a number of the following parameter combinations:

- The matter density parameter combination $\omega_{\rm m} \equiv \Omega_{\rm om} h^2$.
- The baryon density parameter combination $\omega_b \equiv \Omega_{\rm ob} h^2$.
- The radiation density parameter combination $\omega_{\rm r} \equiv \Omega_{\rm or} h^2$.
- The primordial fluctuation spectrum and the curvature parameter $\omega_{\rm k} \equiv \Omega_{\rm ok} h^2$.
- The flat universe co-moving angular diameter distance to the recombination surface

$$d_A(\omega_m, \omega_r, \omega_b, h, w(z)) = \int_0^{z_r} \frac{dz}{H(z)} \tag{3}$$

Where $h = \frac{H_0}{100}\ km\ sec^{-1}\ Mpc^{-1}$, $z_r \approx 1100$ is the recombination redshift and the subscript 0 indicates the present day value of each density parameter.

Efstathiou, G. and Bond, J.R., Mon.Not.Roy.Astron.Soc. 304 (1998) 75-97
Elgaroy, Oystein and Multamaki, Tuomas, Astron. Astrophys. 471 (2007) 65

CMB Spectrum Degeneracies

- By fixing the first four parameter combinations to their Planck18/ΛCDM values, the fifth allows us to analytically predict the value of H_0 for a given dark energy equation of state $w(w_0, w_1, ..., z)$.

CMB Spectrum Degeneracies

- By fixing the first four parameter combinations to their Planck18/ΛCDM values, the fifth allows us to analytically predict the value of H_0 for a given dark energy equation of state $w(w_0, w_1, ..., z)$.
- We can derive the function $h(w_0, w_1, ...)$ if we solve the equation,

$$d_A(\bar{\omega}_m, \bar{\omega}_r, \bar{\omega}_b, h = 0.674, w = -1) = d_A(\bar{\omega}_m, \bar{\omega}_r, \bar{\omega}_b, h, w(z)) \quad (4)$$

where with a bar we symbolize the parameter values as they are determined by the Planck18/ΛCDM power spectrum.

CMB Spectrum Degeneracies

We can show then, that for the wCDM model we will have an $h(w)$ degeneracy function given by the following figure (orange line).

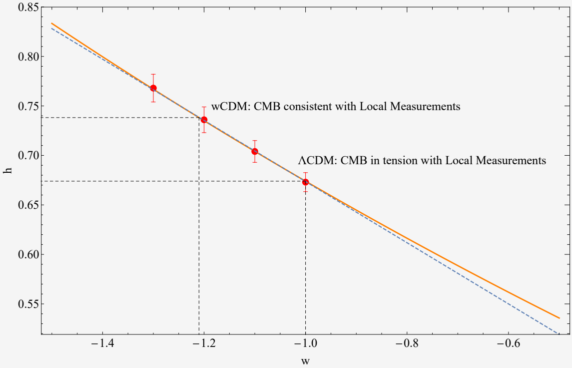

CMB Spectrum Degeneracies

We can show then, that for the wCDM model we will have an $h(w)$ degeneracy function given by the following figure (orange line).

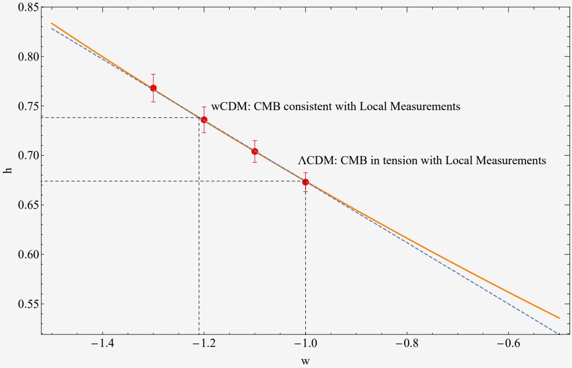

For $w \in [-1.5, -1]$ it is approximately $h(w) \approx -0.3093w + 0.3647$ (dashed blue line).

Numerical Analysis

We test our analytic results as well as their quality of fit compared to ΛCDM.

Numerical Analysis

We test our analytic results as well as their quality of fit compared to ΛCDM.

- We examine the values $w = -1, -1.1, -1.2, -1.3$ and we compare the corresponding best fit values of h and Ω_{0m} obtained analytically, with those given by the Planck TT CMB power spectrum.

Numerical Analysis

We test our analytic results as well as their quality of fit compared to ΛCDM.

- We examine the values $w = -1, -1.1, -1.2, -1.3$ and we compare the corresponding best fit values of h and Ω_{0m} obtained analytically, with those given by the Planck TT CMB power spectrum.

w	Ω_{0m}^{th}	h_{th}	Ω_{0m}^{obs}	h_{obs}	χ^2_{CMB}	$\Delta\chi^2_{CMB}$
-1.0	0.316	0.674	0.315 ± 0.013	0.673 ± 0.010	11266.516	—
-1.1	0.289	0.704	0.288 ± 0.013	0.704 ± 0.011	11266.530	0.014
-1.2	0.265	0.735	$0.263^{+0.012}_{-0.014}$	0.736 ± 0.013	11267.132	0.616
-1.3	0.244	0.766	$0.242^{+0.012}_{-0.013}$	0.768 ± 0.014	11266.520	0.004

Numerical Analysis

The observed values are in excellent agreement with the analytically derived ones, which can also be seen in the following contour plots,

Numerical Analysis

The observed values are in excellent agreement with the analytically derived ones, which can also be seen in the following contour plots,

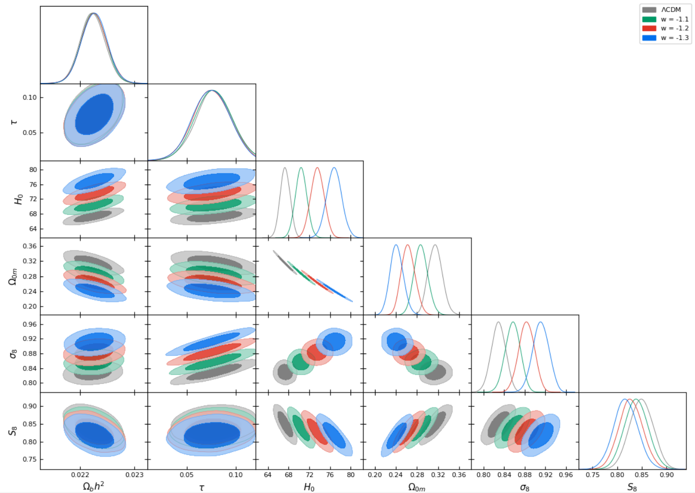

Numerical Analysis

However, when we also include the SnIa and Baryon Acoustic Oscillation (BAO) data,

Numerical Analysis

However, when we also include the SnIa and Baryon Acoustic Oscillation (BAO) data,

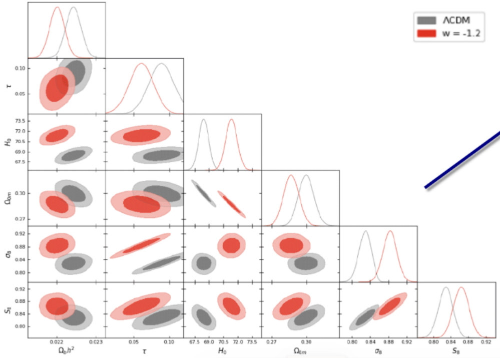

w	χ^2_{tot}	$\Delta\chi^2_{tot}$
-1.0	12319.2	–
-1.2	12332.7	13.5

significantly reduced quality of fit compared to ΛCDM

Numerical Analysis

Unfortunately, while this approach seems to ease the H_0 tension, it does not provide a resolution to the S_8 one, as we can see in the following plots,

Numerical Analysis

Unfortunately, while this approach seems to ease the H_0 tension, it does not provide a resolution to the S_8 one, as we can see in the following plots,

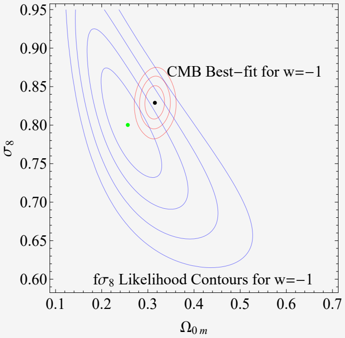

Defining the model

- We propose a parametrization which contains a transition of the SnIa absolute magnitude M at $z_t \in [0.01, 0.1]$ accompanied by transition of the equation dark energy of state parameter $w(z)$ (LwMT).

Defining the model

- We propose a parametrization which contains a transition of the SnIa absolute magnitude M at $z_t \in [0.01, 0.1]$ accompanied by transition of the equation dark energy of state parameter $w(z)$ (LwMT).
- In particular, we consider a transition of $w(z)$ as,

$$w(z) = -1 + \Delta w \, \Theta(z_t - z) \tag{5}$$

coupled with a transition of the SnIa absolute magnitude M of the form,

$$M(z) = M_C + \Delta M \, \Theta(z - z_t) \tag{6}$$

where Θ is the Heaviside step function, $M_C = -19.24$ is the SnIa absolute magnitude calibrated by Cepheids at $z < 0.01$ and ΔM, Δw are parameters to be fit by the data.

G. Alestas, L. Kazantzidis and L. Perivolaropoulos, Phys.Rev.D 103 (2021) 8, 083517
Camarena, David and Marra, Valerio, Phys.Rev.Res. 2 (2020) 1, 013028
G. Alestas, D. Camarena, E. Di Valentino, L. Kazantzidis, V. Marra, S. Nesseris and L. Perivolaropoulos, Phys. Rev. D 105, 063538

Defining the model

- The evolution of dark energy density is

$$\rho_{de}(z) = \rho_{de}(z_p) \int_{z_p}^{z} \frac{dz'}{1+z'} (1 + w(z')) = \rho_{de}(z_p) \left(\frac{1+z}{1+z_p}\right)^{3(1+w)} \tag{7}$$

  where in the last equality a constant w was assumed and z_p is a pivot redshift which may be assumed equal to the present time or equal to the transition time z_t.

- And the Hubble expansion rate $h(z) \equiv H(z)/100\, km\, s^{-1}\, Mpc^{-1}$ takes the form

$$\begin{aligned} h_w(z)^2 &\equiv \omega_m(1+z)^3 + \omega_r(1+z)^4 + (h^2 - \omega_m - \omega_r)\left(\frac{1+z}{1+z_t}\right)^{3\,\Delta w} & z < z_t \\ h_w(z)^2 &\equiv \omega_m(1+z)^3 + \omega_r(1+z)^4 + (h^2 - \omega_m - \omega_r) & z > z_t \end{aligned} \tag{8}$$

Two important conditions to follow

We impose two conditions on the ansantz:

- It should reproduce the comoving distance corresponding to Planck18/ΛCDM r_Λ for $z \gg z_t$ where

$$r_\Lambda(z) \equiv \int_0^z \frac{dz'}{\omega_m(1+z')^3 + \omega_r(1+z')^4 + (h^2 - \omega_m - \omega_r)} \tag{9}$$

  where $\omega_m \equiv \Omega_{0m}h^2 = 0.143$, $\omega_r \equiv \Omega_{0r}h^2 = 4.64 \times 10^{-5}$ and $h = h_{CMB} = 0.674$.

- It should reproduce the local SnIa measurement of the Hubble parameter

$$h_w(z=0) = h_{local} = 0.74 \tag{10}$$

Two important conditions to follow

- The first condition fixes the parameters ω_m, ω_r and h to their Planck18/ΛCDM best fit values.

Two important conditions to follow

- The first condition fixes the parameters ω_m, ω_r and h to their Planck18/ΛCDM best fit values.
- The second condition leads to a relation between Δw and z_t of the form,

$$\Delta w = \frac{Log\left(h^2 - \omega_m\right) - Log\left(h^2_{local} - \omega_m\right)}{3Log(1+z_t)} \tag{11}$$

where $h = h_{CMB} = 0.674$ and $\omega_m = \Omega_{0m}h^2 = 0.143$ as implied by the first condition and for consistency with the CMB anisotropy spectrum.

Comparing comoving distance forms

We compare the form of the comoving distance $r(z)$ predicted in the context of the *LwMT* model $r_w(z)$ with other proposed $H(z)$ deformations for the resolution of the Hubble tension that produce the same CMB anisotropy spectrum as Planck18/ΛCDM while at the same time predict a Hubble parameter equal to its locally measured value $h(z=0) = h_{local}$.

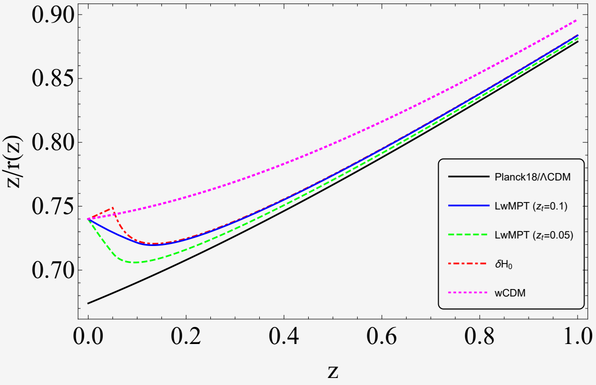

Fitting LwMT to cosmological data

We use the following datasets in order to fit the LwMT, wCDM and ΛCDM models,

Fitting LwMT to cosmological data

We use the following datasets in order to fit the LwMT, wCDM and ΛCDM models,

- The Pantheon SnIa dataset consisting of 1048 distance modulus datapoints in the redshift range $z \in [0.01, 2.3]$.

Fitting LwMT to cosmological data

We use the following datasets in order to fit the LwMT, wCDM and ΛCDM models,

- The Pantheon SnIa dataset consisting of 1048 distance modulus datapoints in the redshift range $z \in [0.01, 2.3]$.
- A compilation of 9 BAO datapoints in the redshift range $z \in [0.1, 2.34]$.

Fitting LwMT to cosmological data

We use the following datasets in order to fit the LwMT, wCDM and ΛCDM models,

- The Pantheon SnIa dataset consisting of 1048 distance modulus datapoints in the redshift range $z \in [0.01, 2.3]$.
- A compilation of 9 BAO datapoints in the redshift range $z \in [0.1, 2.34]$.
- The latest Planck18/ΛCDM CMB distance prior data (shift parameter R and the acoustic scale l_a). These are highly constraining datapoints based on the observation of the sound horizon standard ruler at the last scattering surface $z \simeq 1100$.

Fitting LwMT to cosmological data

We use the following datasets in order to fit the LwMT, wCDM and ΛCDM models,

- The Pantheon SnIa dataset consisting of 1048 distance modulus datapoints in the redshift range $z \in [0.01, 2.3]$.
- A compilation of 9 BAO datapoints in the redshift range $z \in [0.1, 2.34]$.
- The latest Planck18/ΛCDM CMB distance prior data (shift parameter R and the acoustic scale l_a). These are highly constraining datapoints based on the observation of the sound horizon standard ruler at the last scattering surface $z \simeq 1100$.
- A compilation of 41 Cosmic Chronometer (CC) datapoints in the redshift range $z \in [0.1, 2.36]$. (Not very robust!)

Fitting LwMT to cosmological data

- We therefore define χ^2 as

$$\chi^2 = \chi^2_{CMB} + \chi^2_{BAO} + \chi^2_{CC} + \chi^2_{Panth} \tag{12}$$

and calculate the residual $\Delta\chi^2$ with respect to the ΛCDM model for the *LwMT* model (as a function of z_t) and for *wCDM* with $w = -1.22$ and $\omega_m \simeq 0.143$.

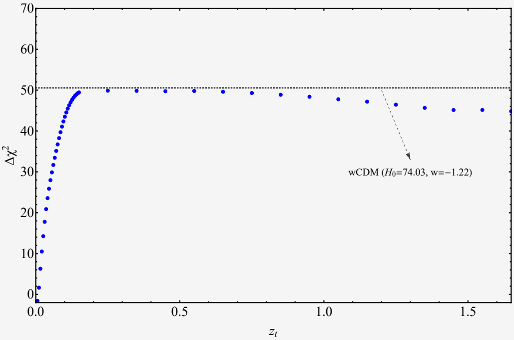

The M transition

- Assuming that that the SnIa absolute luminosity is proportional to the Chandrasekhar mass which varies as $L \sim G_{\rm eff}^{b}$ with $b = -3/2$ we obtain the required evolution of an effective Newton's constant that is required to produce the M transition. This assumption leads to the variation of the SnIa absolute magnitude M with $\mu \equiv \frac{G_{\rm eff}}{G_{\rm N}}$ ($G_{\rm N}$ is the locally measured Newton's constant)

$$\Delta M = \frac{15}{4}\, log_{10}\ (\mu) \tag{13}$$

The M transition

- We present the best fit absolute magnitude M_{bf} (blue points) for various z_t for the *LwMT* model. The dashed line corresponds to the fixed M_C value, while the dot dashed lines correspond its 1σ error.

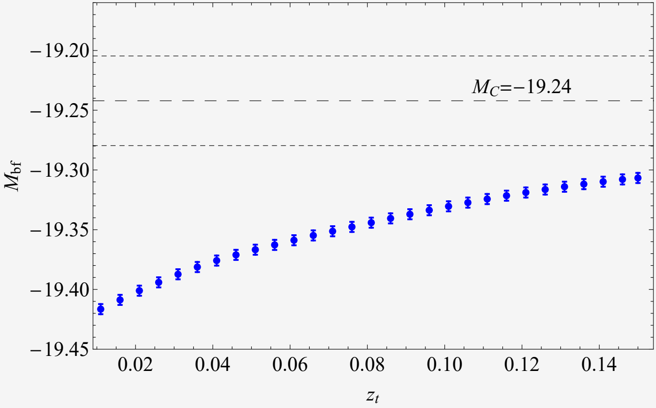

The M transition

- The form of the M transition that is necessary for LwMT to be consistent with the Cepheid absolute magnitude, and the $\mu = G_{\text{eff}}/G_N$ required to induce it are shown below.

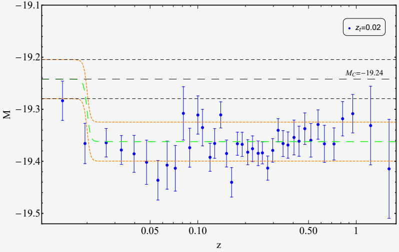

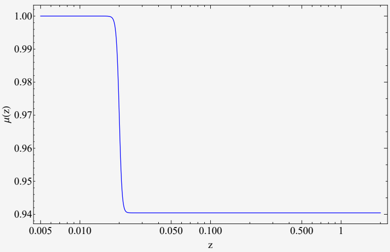

Regarding the S_8 tension

- We have demonstrated by using a generic CPL model that attempts to seemingly solve the H_0 tension that all parametrizations that use late time smooth deformations of the Hubble expansion rate $H(z)$ of the Planck18/ΛCDM best fit, in order to match the locally measured value of H_0 while effectively keeping the comoving distance to the last scattering surface and $\Omega_{0m}h^2$ fixed to maintain consistency with Planck CMB measurements fail to address the growth tension.

Regarding the S_8 tension

- We have demonstrated by using a generic CPL model that attempts to seemingly solve the H_0 tension that all parametrizations that use late time smooth deformations of the Hubble expansion rate $H(z)$ of the Planck18/ΛCDM best fit, in order to match the locally measured value of H_0 while effectively keeping the comoving distance to the last scattering surface and $\Omega_{0m}h^2$ fixed to maintain consistency with Planck CMB measurements fail to address the growth tension.
- In the case of CPL the fact that the tension does not ease is shown by the contours that correspond to the growth and the Plank 18 CMB data, for the ΛCDM and various (w_0, w_1) pairs of the CPL model

Alestas, G. and Perivolaropoulos, L., (2021), Mon.Not.Roy.Astron.Soc. 504 (2021) 3956

Regarding the S_8 tension

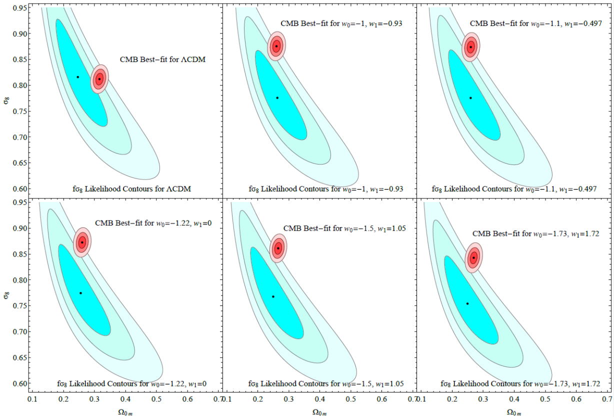

- However in the case of LwMT we expect the growth tension to be improved or at least not be adversely impacted, since it does not fall in the category of smooth $H(z)$ deformations.
Marra, Valerio and Perivolaropoulos, Leandros, Phys.Rev.D 104 (2021) 2, L021303

The evolution of the Tully-Fisher data

- We use an up to date compilation of galaxy data to examine the evolution of the baryonic Tully-Fisher relation (BTFR).

The evolution of the Tully-Fisher data

- We use an up to date compilation of galaxy data to examine the evolution of the baryonic Tully-Fisher relation (BTFR).
- BTFR connects the total baryonic mass of a galaxy (M_B) with its rotation velocity,

$$M_B = A_B v_{rot}^s \tag{14}$$

where $log(A_B)$ is the zero point or intercept in a logarithmic plot, and $s \simeq 4$ is the slope.

The evolution of the Tully-Fisher data

- We use an up to date compilation of galaxy data to examine the evolution of the baryonic Tully-Fisher relation (BTFR).
- BTFR connects the total baryonic mass of a galaxy (M_B) with its rotation velocity,
$$M_B = A_B v_{rot}^s \tag{14}$$
where $log(A_B)$ is the zero point or intercept in a logarithmic plot, and $s \simeq 4$ is the slope.
- A tension in the evolution of BTFR could be attributed to a gravitational transition because,
$$A_B \sim G_{\text{eff}}^{-2} S^{-1} \tag{15}$$
where G_{eff} is the effective Newton's constant and S is the surface density.

The evolution of the Tully-Fisher data

- The logarithmic form of the BTFR is,

$$logM_B = s\, logv_{rot} + \log A_B \equiv s\, y + b \tag{16}$$

The evolution of the Tully-Fisher data

- The logarithmic form of the BTFR is,

$$logM_B = s\, logv_{rot} + \log A_B \equiv s\, y + b \tag{16}$$

- We can see that the intercept of the line is connected with the strength of the gravitational interactions.

The evolution of the Tully-Fisher data

- The logarithmic form of the BTFR is,

$$logM_B = s\,logv_{rot} + \log A_B \equiv s\,y + b \tag{16}$$

- We can see that the intercept of the line is connected with the strength of the gravitational interactions.
- While studies of the evolution of BTFR have been done in the past, none of them has focused at searching for abrupt transitions of the intercept or slope values at very low redshifts.

The evolution of the Tully-Fisher data

- The logarithmic form of the BTFR is,

$$logM_B = s\, logv_{rot} + \log A_B \equiv s\, y + b \tag{16}$$

- We can see that the intercept of the line is connected with the strength of the gravitational interactions.
- While studies of the evolution of BTFR have been done in the past, none of them has focused at searching for abrupt transitions of the intercept or slope values at very low redshifts.

That is exactly what we did.
G. Alestas, I. Antoniou and L. Perivolaropoulos, Universe 7 (2021) 366

The evolution of the Tully-Fisher data

- We consider the BTFR dataset of the updated SPARC database consisting of the distance D, the logarithm of the baryonic mass $\log M_B$ and the logarithm of the asymptotically flat rotation velocity $\log v_{rot}$ of 118 galaxies along with their 1σ errors.

The main characteristics of our study is that,

The evolution of the Tully-Fisher data

- We consider the BTFR dataset of the updated SPARC database consisting of the distance D, the logarithm of the baryonic mass $\log M_B$ and the logarithm of the asymptotically flat rotation velocity $\log v_{rot}$ of 118 galaxies along with their 1σ errors.

The main characteristics of our study is that,

- We use an exclusively low z sample of data.

The evolution of the Tully-Fisher data

- We consider the BTFR dataset of the updated SPARC database consisting of the distance D, the logarithm of the baryonic mass $\log M_B$ and the logarithm of the asymptotically flat rotation velocity $\log v_{rot}$ of 118 galaxies along with their 1σ errors.

The main characteristics of our study is that,

- We use an exclusively low z sample of data.
- We focus on a particular type of evolution, sharp transitions of the intercept and slope.

The evolution of the Tully-Fisher data

- We fix a critical distance D_c and split our sample in two subsamples Σ_1 (galaxies with $D < D_c$) and Σ_2 (galaxies with $D > D_c$).

The evolution of the Tully-Fisher data

- We fix a critical distance D_c and split our sample in two subsamples Σ_1 (galaxies with $D < D_c$) and Σ_2 (galaxies with $D > D_c$).
- For each subsample we use the maximum likelihood method and perform a linear fit to the data setting $y_i = \log(M_B)_i$, $x_i = \log(v_{rot})_i$ while the parameters to fit are the slope and the intercept.

The evolution of the Tully-Fisher data

- We fix a critical distance D_c and split our sample in two subsamples Σ_1 (galaxies with $D < D_c$) and Σ_2 (galaxies with $D > D_c$).
- For each subsample we use the maximum likelihood method and perform a linear fit to the data setting $y_i = \log(M_B)_i$, $x_i = \log(v_{rot})_i$ while the parameters to fit are the slope and the intercept.
- Therefore, for each sample j ($j = 0, 1, 2$ with $j = 0$ corresponding to the full sample and $j = 1, 2$ corresponding to the two subsamples Σ_1 and Σ_2) we attempt to minimize,

$$\chi_j^2(s, b) = \sum_{i=1}^{N_j} \frac{\left[y_i - (s_j\, x_i + b_j)\right]^2}{s_j^2 + \sigma_{xi}^2 + \sigma_{yi}^2 + \sigma_s^2} \tag{17}$$

with respect to the slope s_j and intercept b_j.

The evolution of the Tully-Fisher data

Plotting the σ-distance between the each pair of subsamples as a function of the split distance D_c we observe two statistically significant abrupt peaks at $9Mpc$ and $17Mpc$.

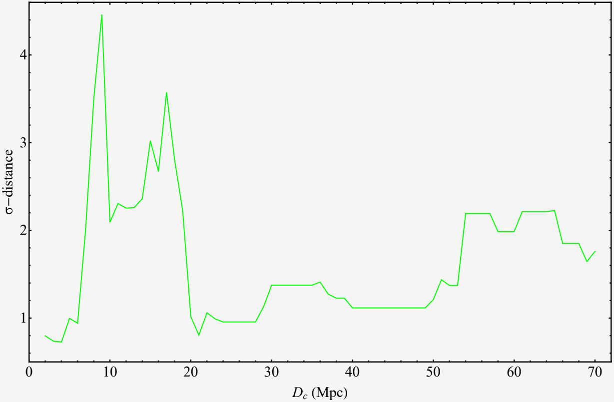

G_{eff} constraints from low-z galaxy survey data

- We search for a shift in the Hubble expansion rate at $z < 0.01$ caused by a transition of the G_{eff}.

$G_{\rm eff}$ constraints from low-z galaxy survey data

- We search for a shift in the Hubble expansion rate at $z < 0.01$ caused by a transition of the $G_{\rm eff}$.
- It could be detectable indirectly as a signal in the observed number of galaxies per redshift bin at $z < 0.01$.

G_{eff} constraints from low-z galaxy survey data

- We search for a shift in the Hubble expansion rate at $z < 0.01$ caused by a transition of the G_{eff}.
- It could be detectable indirectly as a signal in the observed number of galaxies per redshift bin at $z < 0.01$.
- In the context of the scalar-tensor modified gravity theories the Friedman equation in redshift space may be expressed as

$$H(z)^2 = \frac{8\pi G_{\text{eff}}(z)}{3}\rho_{tot} \tag{18}$$

where ρ_{tot} refers to the total energy density including matter and an effective geometric dark energy component induced *e.g.* by the non-minimally coupled scalar field.

$G_{\rm eff}$ constraints from low-z galaxy survey data

- We search for a shift in the Hubble expansion rate at $z < 0.01$ caused by a transition of the $G_{\rm eff}$.
- It could be detectable indirectly as a signal in the observed number of galaxies per redshift bin at $z < 0.01$.
- In the context of the scalar-tensor modified gravity theories the Friedman equation in redshift space may be expressed as

$$H(z)^2 = \frac{8\pi G_{\rm eff}(z)}{3}\rho_{tot} \tag{18}$$

  where ρ_{tot} refers to the total energy density including matter and an effective geometric dark energy component induced *e.g.* by the non-minimally coupled scalar field.
- So a change of $G_{\rm eff}$ at z_t would also lead to a corresponding abrupt change of $H(z)$ such that

$$\frac{\Delta G_{\rm eff}}{G_{\rm eff}} = 2\frac{\Delta H}{H}. \tag{19}$$

G_{eff} constraints from low-z galaxy survey data

- Using galaxy redshift surveys at $z < 0.01$ it is possible to bin the observed galaxies in redshift bins of width Δz such that there are $\Delta N(z_i)$ galaxies in the i bin.

G_{eff} constraints from low-z galaxy survey data

- Using galaxy redshift surveys at $z < 0.01$ it is possible to bin the observed galaxies in redshift bins of width Δz such that there are $\Delta N(z_i)$ galaxies in the i bin.
- In the presence of random peculiar velocities the measured redshift of a given galaxy may be written as $cz = H_0 s + c\Delta z_r$, where H_0 is the Hubble expansion rate at the galactic distance s and $c\Delta z_r$ is a perturbation due to peculiar velocity effects and may be approximated to have random Gaussian distribution $(\mu = 0,\ \sigma = 300\,\text{km s}^{-1})$.

$G_{\rm eff}$ constraints from low-z galaxy survey data

- Using galaxy redshift surveys at $z < 0.01$ it is possible to bin the observed galaxies in redshift bins of width Δz such that there are $\Delta N(z_i)$ galaxies in the i bin.
- In the presence of random peculiar velocities the measured redshift of a given galaxy may be written as $cz = H_0 s + c\Delta z_r$, where H_0 is the Hubble expansion rate at the galactic distance s and $c\Delta z_r$ is a perturbation due to peculiar velocity effects and may be approximated to have random Gaussian distribution $(\mu = 0,\ \sigma = 300\,\mathrm{km\,s^{-1}})$.
- The number of galaxies that exist in a spherical shell with radius s is given by $N(s) = \frac{4\pi}{3} s^3 \rho(z)$, where we approximate the density at the redshift $\rho(z) = \rho_0 (1+z)^3 \approx \rho_0$ as homogeneous.

G_{eff} constraints from low-z galaxy survey data

- Using galaxy redshift surveys at $z < 0.01$ it is possible to bin the observed galaxies in redshift bins of width Δz such that there are $\Delta N(z_i)$ galaxies in the i bin.
- In the presence of random peculiar velocities the measured redshift of a given galaxy may be written as $cz = H_0 s + c\Delta z_r$, where H_0 is the Hubble expansion rate at the galactic distance s and $c\Delta z_r$ is a perturbation due to peculiar velocity effects and may be approximated to have random Gaussian distribution $(\mu = 0,\ \sigma = 300\,\mathrm{km\,s^{-1}})$.
- The number of galaxies that exist in a spherical shell with radius s is given by $N(s) = \frac{4\pi}{3}s^3\rho(z)$, where we approximate the density at the redshift $\rho(z) = \rho_0(1+z)^3 \approx \rho_0$ as homogeneous.
- So the number of galaxies in the i redshift bin takes the form

$$\Delta N(z_i) = 4\pi\rho_0 \left(\frac{c}{H_0}\right)^3 (z_i - \Delta z_r)^2 \Delta z_i \tag{20}$$

where Δz_i is width of the i redshift bin assumed to be the same for all bins.

$G_{\rm eff}$ constraints from low-z galaxy survey data

- Therefore, the predicted number of galaxies in the i bin $\Delta N(z_i)$ is related to the number of galaxies in the $j = 1$ bin as

$$\Delta N(z_i) = \Delta N(z_1) \left(\frac{cz_i - c\Delta z_r}{cz_1 - c\Delta z_r} \right)^2 \left(\frac{H_{01}}{H_{0i}} \right)^3 \tag{21}$$

G_{eff} constraints from low-z galaxy survey data

- Therefore, the predicted number of galaxies in the i bin $\Delta N(z_i)$ is related to the number of galaxies in the $j = 1$ bin as

$$\Delta N(z_i) = \Delta N(z_1) \left(\frac{cz_i - c\Delta z_r}{cz_1 - c\Delta z_r} \right)^2 \left(\frac{H_{01}}{H_{0i}} \right)^3 \tag{21}$$

- Eq. (21) allows for a transition in the Hubble diagram slope H_0 at some redshift z_t. Such a transition could be expressed as

$$H_{0i} = H_{01} - \Delta H_0 \Theta(z_i - z_t) \tag{22}$$

G_{eff} constraints from low-z galaxy survey data

- Therefore, the predicted number of galaxies in the i bin $\Delta N(z_i)$ is related to the number of galaxies in the $j = 1$ bin as

$$\Delta N(z_i) = \Delta N(z_1) \left(\frac{cz_i - c\Delta z_r}{cz_1 - c\Delta z_r} \right)^2 \left(\frac{H_{01}}{H_{0i}} \right)^3 \tag{21}$$

- Eq. (21) allows for a transition in the Hubble diagram slope H_0 at some redshift z_t. Such a transition could be expressed as

$$H_{0i} = H_{01} - \Delta H_0 \Theta(z_i - z_t) \tag{22}$$

- In this case eq. (21) takes the form

$$\Delta N(A, \delta, z_t, z_i) = A \left(\frac{cz_i - c\Delta z_r}{cz_1 - c\Delta z_r} \right)^2 \left[1 - \delta\ \Theta(z_i - z_t)\right]^{-3} \tag{23}$$

where $A \simeq \Delta N(z_1)$ and $\delta \equiv \frac{\Delta H_0}{H_0}$ are parameters to be fitted by survey data.

G_{eff} constraints from low-z galaxy survey data

- We implement the maximum likelihood method by minimizing χ^2 with respect to the parameters A, $\delta \equiv \frac{\Delta H_0}{H_0}$ and z_t.

G_{eff} constraints from low-z galaxy survey data

- We implement the maximum likelihood method by minimizing χ^2 with respect to the parameters A, $\delta \equiv \frac{\Delta H_0}{H_0}$ and z_t.
- We minimize

$$\chi^2(A, \delta, z_t) = \sum_{i=1}^{N_{tot}} \frac{[\Delta N(z_i)_{dat} - \Delta N(A, \delta, z_t, z_i)]^2}{\sigma_i^2 + \sigma_s^2} \tag{24}$$

where N_{tot} is the total number of bins, $\sigma_i^2 = N_{tot}/\Delta N(z_i)_{dat}$ is the Poisson distribution error for each bin and σ_s is the scatter error fixed such that the minimum χ^2_{min} per degree of freedom is equal to one.

$G_{\rm eff}$ constraints from low-z galaxy survey data

- We implement the maximum likelihood method by minimizing χ^2 with respect to the parameters A, $\delta \equiv \frac{\Delta H_0}{H_0}$ and z_t.
- We minimize

$$\chi^2(A,\delta,z_t) = \sum_{i=1}^{N_{tot}} \frac{[\Delta N(z_i)_{dat} - \Delta N(A,\delta,z_t,z_i)]^2}{\sigma_i^2+\sigma_s^2} \tag{24}$$

  where N_{tot} is the total number of bins, $\sigma_i^2 = N_{tot}/\Delta N(z_i)_{dat}$ is the Poisson distribution error for each bin and σ_s is the scatter error fixed such that the minimum χ^2_{min} per degree of freedom is equal to one.
- We use 2 low-z galaxy survey datasets, 6dFGS and 2MRS.

$G_{\rm eff}$ constraints from low-z galaxy survey data

Both for the 6dFGS (red) and the 2MRS (magenta) datasets we can see a peak/dip feature in the redshift space number density of galaxies, as shown in the following histograms,

$G_{\rm eff}$ constraints from low-z galaxy survey data

Both for the 6dFGS (red) and the 2MRS (magenta) datasets we can see a peak/dip feature in the redshift space number density of galaxies, as shown in the following histograms,

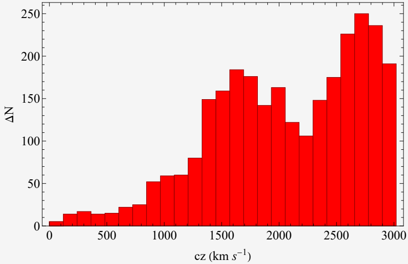

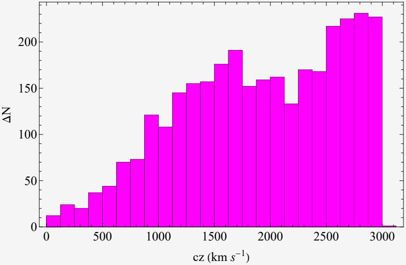

$G_{\rm eff}$ constraints from low-z galaxy survey data

- Assuming that the gravitational transition is the only cause of the observed dip in the $\Delta N(z)$ distribution we minimize χ^2 (eq. (24)) obtaining the best fit parameters A, δ and z_t.

G_{eff} constraints from low-z galaxy survey data

- Assuming that the gravitational transition is the only cause of the observed dip in the $\Delta N(z)$ distribution we minimize χ^2 (eq. (24)) obtaining the best fit parameters A, δ and z_t.
- Such a fit for $\delta \equiv \Delta H_0/H_0$ should be interpreted as an upper bound for the transition amplitude δ and therefore also for the gravitational transition amplitude.

$G_{\rm eff}$ constraints from low-z galaxy survey data

- Assuming that the gravitational transition is the only cause of the observed dip in the $\Delta N(z)$ distribution we minimize χ^2 (eq. (24)) obtaining the best fit parameters A, δ and z_t.
- Such a fit for $\delta \equiv \Delta H_0/H_0$ should be interpreted as an upper bound for the transition amplitude δ and therefore also for the gravitational transition amplitude.
- For the 6dFGS data we obtain the best fit parameter values as $cz_t \approx 1810 \pm 150\,\mathrm{km\,s^{-1}}$, $A = 20.9 \pm 0.5$ and $\delta = \frac{\Delta H_0}{H_0} = -0.275 \pm 0.01$ for a fixed value of $\sigma_s \approx 3.7$.

G_{eff} constraints from low-z galaxy survey data

- Assuming that the gravitational transition is the only cause of the observed dip in the $\Delta N(z)$ distribution we minimize χ^2 (eq. (24)) obtaining the best fit parameters A, δ and z_t.
- Such a fit for $\delta \equiv \Delta H_0 / H_0$ should be interpreted as an upper bound for the transition amplitude δ and therefore also for the gravitational transition amplitude.
- For the 6dFGS data we obtain the best fit parameter values as $cz_t \approx 1810 \pm 150\,\text{km s}^{-1}$, $A = 20.9 \pm 0.5$ and $\delta = \frac{\Delta H_0}{H_0} = -0.275 \pm 0.01$ for a fixed value of $\sigma_s \approx 3.7$.
- For the 6dFGS data we obtain the best fit parameter values as $A = 17.5 \pm 0.5$, $\delta = \frac{\Delta H_0}{H_0} = -0.28 \pm 0.01$ and $cz_t \approx 1783 \pm 150$ km s^{-1} for $\sigma_s \approx 3.4$.

$G_{\rm eff}$ constraints from low-z galaxy survey data

- Assuming that the gravitational transition is the only cause of the observed dip in the $\Delta N(z)$ distribution we minimize χ^2 (eq. (24)) obtaining the best fit parameters A, δ and z_t.
- Such a fit for $\delta \equiv \Delta H_0/H_0$ should be interpreted as an upper bound for the transition amplitude δ and therefore also for the gravitational transition amplitude.
- For the 6dFGS data we obtain the best fit parameter values as $cz_t \approx 1810 \pm 150\,\text{km s}^{-1}$, $A = 20.9 \pm 0.5$ and $\delta = \frac{\Delta H_0}{H_0} = -0.275 \pm 0.01$ for a fixed value of $\sigma_s \approx 3.7$.
- For the 6dFGS data we obtain the best fit parameter values as $A = 17.5 \pm 0.5$, $\delta = \frac{\Delta H_0}{H_0} = -0.28 \pm 0.01$ and $cz_t \approx 1783 \pm 150\,\text{km s}^{-1}$ for $\sigma_s \approx 3.4$.
- These lead to a $\frac{\Delta G_{\rm eff}}{G_{\rm eff}} \lesssim 0.6$.

$G_{\rm eff}$ constraints from low-z galaxy survey data

- Although we have shown, via the Cosmological Lofty Realizations (CoLoRe) package, that the effect most likely is due to galactic density fluctuations or coherent peculiar velocities of galaxies, an ultra late time gravitational transition cannot be fully excluded.

G_{eff} constraints from low-z galaxy survey data

- Although we have shown, via the Cosmological Lofty Realizations (CoLoRe) package, that the effect most likely is due to galactic density fluctuations or coherent peculiar velocities of galaxies, an ultra late time gravitational transition cannot be fully excluded.
- At the very least we have shown that the gravitational transition hypothesis cannot be ruled out by redshift survey data at $z < 0.01$.

G. Alestas, L. Perivolaropoulos and K. Tanidis, ArXiv: 2201.05846 [astro-ph.CO]

Summary

- We have stated a problem at the heart of the Hubble tension. The fact that it also concerns the SnIa absolute magnitude M.

Summary

- We have stated a problem at the heart of the Hubble tension. The fact that it also concerns the SnIa absolute magnitude M.
- We have shown that an H_0 - $w(z)$ degeneracy that is inherent in the CMB power spectrum can be used in order to seemingly resolve the H_0 tension, worsening however the S_8 tension.

Summary

- We have stated a problem at the heart of the Hubble tension. The fact that it also concerns the SnIa absolute magnitude M.
- We have shown that an H_0 - $w(z)$ degeneracy that is inherent in the CMB power spectrum can be used in order to seemingly resolve the H_0 tension, worsening however the S_8 tension.
- We have demonstrated how, at least in principle, a late time transition model could provide a resolution to the Hubble crisis. This model constitutes of a transition in the dark energy equation of state w coupled with an absolute magnitude M transition which is translated to a gravitational transition.

Summary

- We have stated a problem at the heart of the Hubble tension. The fact that it also concerns the SnIa absolute magnitude M.
- We have shown that an H_0 - $w(z)$ degeneracy that is inherent in the CMB power spectrum can be used in order to seemingly resolve the H_0 tension, worsening however the S_8 tension.
- We have demonstrated how, at least in principle, a late time transition model could provide a resolution to the Hubble crisis. This model constitutes of a transition in the dark energy equation of state w coupled with an absolute magnitude M transition which is translated to a gravitational transition.
- We have also given observational evidence supporting a such gravitational transition, while we attempted to constrain it. The former was done using the evolution of the baryonic Tully-Fisher relation and the latter using two low-z redshift survey datasets.

Looking Ahead

- Although it works in principle, the *LwMT* model seems to require a degree of fine-tuning.

Looking Ahead

- Although it works in principle, the *LwMT* model seems to require a degree of fine-tuning.
- Can we construct a simple and intuitive modified gravity model, that could naturally induce the gravitational transition predicted by *LwMT*?

Looking Ahead

- Although it works in principle, the *LwMT* model seems to require a degree of fine-tuning.
- Can we construct a simple and intuitive modified gravity model, that could naturally induce the gravitational transition predicted by *LwMT*?
- Could there be any other physical mechanisms, other than the gravitational transition one, that would motivate a SnIa absolute magnitude transition?

Looking Ahead

- Although it works in principle, the *LwMT* model seems to require a degree of fine-tuning.
- Can we construct a simple and intuitive modified gravity model, that could naturally induce the gravitational transition predicted by *LwMT*?
- Could there be any other physical mechanisms, other than the gravitational transition one, that would motivate a SnIa absolute magnitude transition?
- Other astrophysical relations that involve gravitational physics like the Faber-Jackson relation between intrinsic luminosity and velocity dispersion of elliptical galaxies or the Cepheid star period-luminosity relation could also be screened for similar types of transitions as in the case of BTFR.

Thank you!!

Guest Stars!

H_0 Measurements

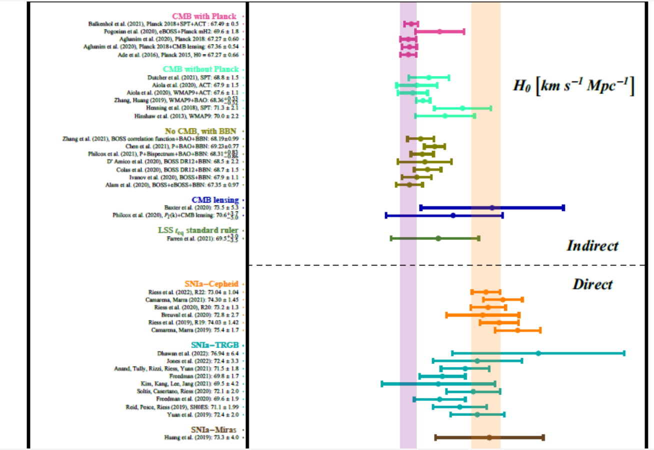

H_0 Measurements

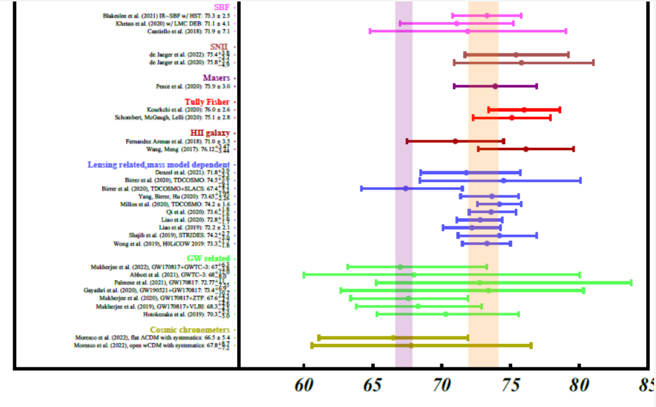

SHoES distance ladder

The intercept α_B of the Hubble law has the form

$$\alpha_B = \log cz \left[1 + \frac{1}{2}(1 - q_0)z - \frac{1}{6}(1 - q_0 - 3q_0^2 + j_0)z^2 + O(z^3)\right] - 0.2m_B^0 \tag{25}$$

and can give us H_0 via $\log H_0 = 0.2M_B^0 + \alpha_B + 5$.

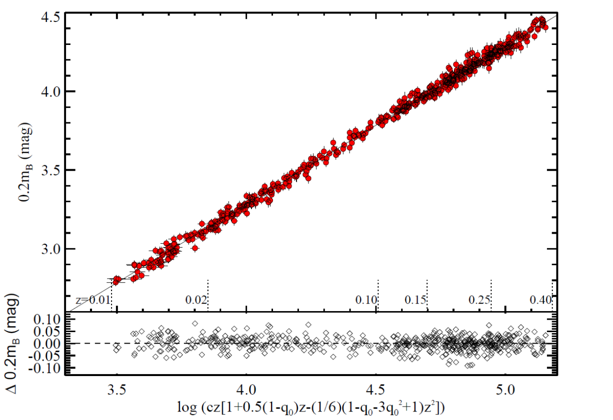

Fitting LwMT to cosmological data

- We show the difficulty of the smooth $H(z)$ deformation models that address the Hubble tension in fitting the BAO and SnIa data. We show the BAO and SnIa data (residuals from the best fit ΛCDM) along with the best fit residuals for the *wCDM* and *LwMT* models.

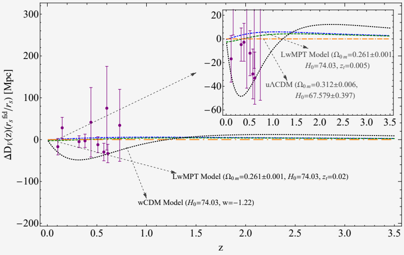

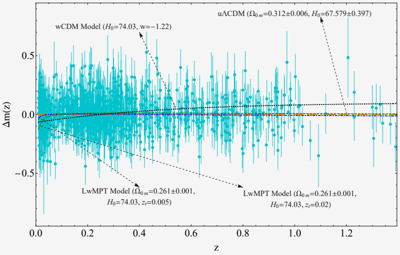

The evolution of the Tully-Fisher data

- By demanding that $\frac{\chi^2_{0,min}}{N_0} = 1$ we fix the scatter to $\sigma_s = 0.077$, where $\chi^2_{0,min}$ is the minimized value of χ^2 for the full sample and N_0 is the number of data points of the full sample.
- We thus find the best fit values of the parameters s_j and b_j, $(j = 0, 1, 2)$.
- We then evaluate the $\Delta\chi^2_{kl}(D_c)$ of the best fit of each subsample k with respect to the likelihood contours of the other subsample l. Using these values we also evaluate the σ-distances ($d_{\sigma,kl}(D_c)$ and $d_{\sigma,lk}(D_c)$) and conservatively define the minimum of these σ-distances as,

$$d_\sigma(D_c) \equiv Min\left[d_{\sigma,12}(D_c), d_{\sigma,21}(D_c)\right] \tag{26}$$

The evolution of the Tully-Fisher data

In order to make sure that our results are not biased due to not taking into account the uncertainties in the galactic distances we have repeated the analysis using Monte Carlo simulations of 100 samples with randomly varying galaxy distances. The distance to each galaxy in each random sample varied randomly with a Gaussian distribution with mean equal to the measured distance and standard deviation equal to the corresponding 1σ error. The results of this analysis are shown in the following figure,

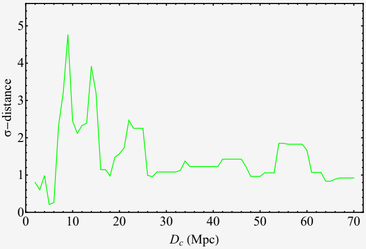

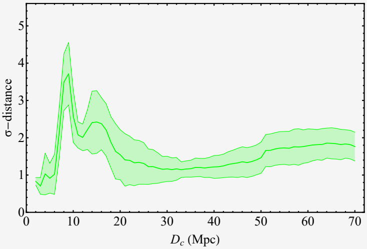

The evolution of the Tully-Fisher data

These are the best fit $logM_B - logv_{rot}$ lines for selected galactic subsamples superimposed with the datapoints. The difference between the two lines for $D_c = 9Mpc$ and $D_c = 17Mpc$ is evident even though their slopes are very similar.